energies

MDPI

Article

An Eulerian Two-Fluid Model Computation Strategy of Alkaline Water Electrolysis for Hydrogen Production

Damien Le Bideau[1], Philippe Mandin[2]* and Mohamed Benbouzid[3], Myeongsub Kim[4], Mathieu Sellier[5], Fabrizio Ganci[6], Rosalinda Inguanta[7]

[1] Institut de Recherche Dupuy de Lôme (UMR CNRS 6027 IRDL), University Bretagne Sud, 56100 Lorient, France; damien.le-bideau@univ-ubs.fr (D.L.B.); philippe.mandin@univ-ubs.fr (P.M.)
[2] Institut de Recherche Dupuy de Lôme (UMR CNRS 6027 IRDL), University of Brest, 29238 Brest, France; Mohamed.Benbouzid@univ-brest.fr (M.B.)
[3] Department of Ocean and Mechanical Engineering, Florida Atlantic University, Boca Raton, USA, kimm@fau.edu (M.K.)
[4] Department of Mechanical Engineering, University of Canterbury, Christchurch 8140, New Zealand, mathieu.sellier@canterbury.ac.nz (M.S.)
[5] Dipartimento di Ingegneria, University of Palermo, Viale delle Scienze, Palermo, 90128, Italy; fabrizio.ganci@unipa.it F.G.); rosalinda.inguanta@unipa.it (R.I.)

* Corresponding author: Mohamed.Benbouzid@univ-brest.fr

Received: date; Accepted: date; Published: date

Abstract: Hydrogen storage is a promising technology for storage of renewable energy resources. Despite its high energy density potential, the development of hydrogen storage has been impeded due mainly to its significant cost. Although its price is governed mainly by electrical energy price, especially for hydrogen produced with alkaline water electrolysis, the price is also driven by value of the cell tension. The most common means of improvement is the use of an electrocatalyst which reduces the energy required for the electrochemical reaction to take place. Another interesting way of electrolyzers improvement is to use the CFD (Computational Fluid Dynamics) assisted design that allow the comprehension of the phenomena occurring in the electrolyzer and also the improvement of the electrolyzer's efficiency. In the present study, a two-phases hydrodynamics model has been defined and computational results are compared with the experimental results of velocity profiles measured using Laser Doppler Velocimetry (LDV) ethod. We found that the CFD results were in good agreement with the experimental data. Under the good fit with experimental values, it is efficient to introduce a new physical bubble transfer phenomenon description called "bubble diffusion".

Keywords: Hydrogen production, Alkaline water electrolysis; Two-phases flow ; CFD ; Two-phase process

1. Introduction

A key challenge of the 21st century is to deal with climate change. The IPCC (Intergovernmental Panel on Climate Change) declares that to stay below the 3°C of global temperature increase from the pre-industrial era a no net emission of greenhouse gases must be achieved at the mid-century. Thus, consumption of fossil-based fuels must be reduced as much as possible. The present global energy demands can hardly be met simply by replacing conventional fossil-based energy sources (e.g., thermal or nuclear) by renewable ones. The integration of renewables into the national electrical grid brings the issue of energy storage because of the intermittent nature of renewable energy resources. Energy storage is achieved using several processes such as battery, STEP or super capacitor.

However, only a few processes allow interseasonal storage (synthetic natural gas and hydrogen (H_2)) and only electrolytic H_2 does not emit greenhouse gases. Electrolytic hydrogen is a promising storage technology due to its high specific potential energy and storage time, but its cost hampers its development. There exist three leading electrolysis technologies, but only two has been employed in industrial applications: they are the alkaline and PEM (Proton Exchange Membrane) electrolyzer. The latter is more efficient than the former but due to the requirement of acidic electrolyte, rare materials must be used (such as platinum). Alkaline water electrolyzer has several advantages over PEM electrolyzer such as its robustness, cheaper costs, and mature. One way of decreasing the cost is to increase the efficiency of the process by decreasing the cell voltage. The cell voltage is a sum of overvoltage Equation (1).

$$U_{cell}(j) = E_{rev}(P,T) + \eta(j)_{cath\ act} + \eta(j)_{an\ act} + R(T,\ Y_{KOH})\ \ j + \eta(j)_{cath\backslash an\ conc} \quad (1)$$

E_{rev} is the reversible voltage in V, η_{act} is the activation overvoltage in V, R the sum of the electrodes, membrane and electrolyte resistance in Ω cm^{-2} and η_{conc} the concentration overpotential in V, j the current density in A m^{-2}.

The E_{rev} voltage represents the minimum voltage where the water electrolysis occurs. This value is around 1.23V at atmospheric pressure and 25°C. This minimal voltage can be decreased by increasing the temperature. The majority of previous studies have focused on finding a cheap, robust and electroactive electrode materials to decrease the activation overpotential, which is the second term of the Equation (1) [1–3]. Another way of increasing the efficiency is to decrease the ohmic resistance through the electrolyzer design using simulations or experiments. Even if it is theoretically possible to perform monophasic alkaline water electrolysis [4], this process is performed under two-phase flow configuration in the industry. Thus, the bubble impact on the efficiency must be modelled or simulated. The first well- known study about this subject was performed by Tobias *et al.* [5] and Hine *et al.* [6]. Both studies focused on the bubble effect on the electrolyte resistance. More recently, the simulation has been used to study this two-phase flow phenomenon. There are two main models: Euler-Euler and Euler-Lagrange models. The latter considers the electrolyte as continua phase and the bubbles as a discrete phase. Mandin *et al.* [7] used this model in their study that the bubble dispersion is taking into account using a horizontal source term. Hreiz *et al.* [8] also used this model. In order to prevent the use of the source term, the bubble injection has been shifted away from electrodes surfaces. Using this technique, it has been concluded that the drag force was sufficient to describe the bubble-liquid interaction. However, the presented comparison with the experiments in their study was mainly qualitative. For Euler-Euler models, two types of models have been used: the mixture model and the two-fluid model, the former has been employed by Dahlkild [9], Wedin *et al.* [10] and Schillings [11]. In those three studies, the model used is called as semi-empirical because empirical correlation is chosen. In Wedin *et al.*[10] and Schillings [11], the calculation are compared to the experiments performed by Boissonneau *et al.*[12]. Those models prevent the use of turbulence closing model. However, Boissonneau *et al.* [12] observed a bubble induced turbulent behavior in the upper part of the narrow and small electrochemical cell. In their study, Aldas *et al.* [13] used a laminar two-fluid model and found that this model underestimates the void fraction distribution compared to the experiment. They concluded that local weak turbulence must be taking into account. In another study, Mat [14] developed a two-fluid model that takes into account local turbulence. The computed results were compared with the experimental void fraction distribution results of Riegel [15] and good agreements were found. In this study, a two-fluid Euler-Euler is developed and will be compared with the experimental results of Boissonneau *et al.* [12] and the numerical results of Schillings[11].

2. Numerical Methods

This section describes the geometry and the type of mesh used in the current study. The mathematical formulation, the boundary conditions, the numerical procedure are also introduced.

Comparison of the numerical results with the experiments and discussion will be followed in the next section.

2.1. Geometry and mesh

The geometry of the computational domain is identical to the experimental apparatus of Boissonneau *et al.* [12]. It is composed of a channel with a height of 120mm, a width of 3mm and a thickness of 30mm. The whole channel is submerged in the electrolyte. The electrodes are 40mm high and are placed 40mm away from the bottom. When the current is applied, bubbles are generated at electrode surfaces. The detached bubbles rise and trigger the electrolyte causing the pumping of the surrounding electrolyte. This phenomenon is called gas-lift configuration.

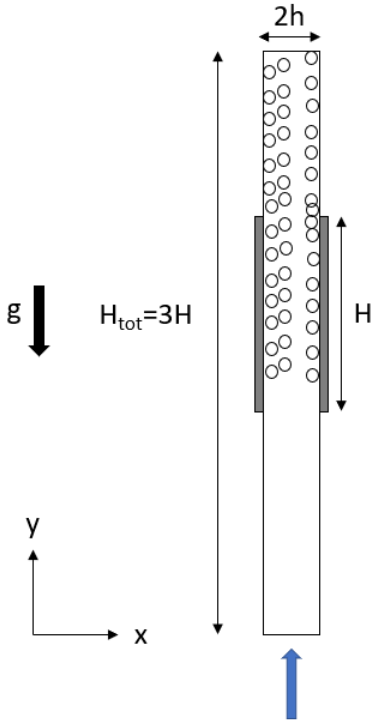

Figure 1. Geometry of the computation domain. h stands for the half-width of the electrolyte, H for the electrode height, L for the cell thickness. The blue arrow symbolizes the pumping electrolyte induced by the electrogenerated bubbles.

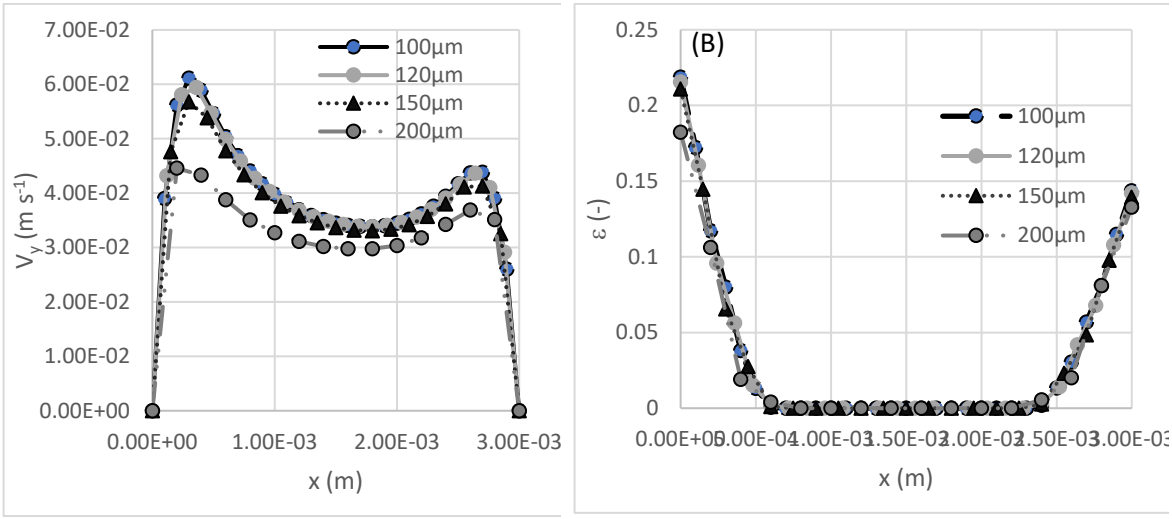

Figure 2. Results of the mesh sensitivity study. The graph (a) presents the mesh dependence of the velocity. The graph (b) presents the mesh dependence of the void fraction.

In numerical calculation, a grid sensitivity study must be performed in order to obtain a grid-independent solution. In this study, the grid is refined until the difference between two solutions reaches zero. However, in 2D two-fluid model, this is not always possible. Indeed, Picardi *et al.* [16] suggested that there is an ideal grid resolution for the two-dimensional two-fluid model simulation. They determined that the grid resolution must respect the bubble-to-cell ratio $1/\sqrt{2}$. If a finer grid is chosen, the results become non-physical or the calculations diverge The same results have been reproduced by Law *et al.* [17]. Finally, Picardi *et al.* [18] stated that this problem is disappeared when a 3D geometry was employed. Nevertheless, their calculation took more time than in 2D (from 10CPU hours to 94 days). Panicker *et al.* [18] and Vaidheeswaran *et al.* [19] explained this phenomenon by the fact that the problem is ill-posed. An iIll-posed problem means that the solution is elliptic. The solution of the Nth step depends on the N+1th step. They solved the problem by adding a collision or dispersion term. They also affirmed that although the virtual mass force has an insignificant influence on the results, it ensures a better stability on the calculation. Panicker *et al.* [18] declared that other authors solved this problem by artificially increasing the liquid viscosity or adding an interface pressure term to the model. Both articles used a linear stability analysis and using the results of this study, Panicker *et al.* [18] added a dispersion term that uses the void fraction gradient. To ensure the hyperbolicity, a parameter depending on the void fraction has been added to the dispersion term. As a result, the resulting model gives better results when compared with the model without the dispersion term. In this study, we choose to add the dispersion term used in studies by Marfaing *et al.* [20] and Davidson[21]. The Figure 2 shows the results of the grid sensitivity. Four size meshes: 100, 120, 150 and 200µm. It can be noted that there is a discrepancy of around 10% in the all domains with the grid size between a 200µm and a 150µm. The maximum difference between the 150µm grid and the other grids are located at the velocity and void fraction peaks. Even if it seems that 100µm is sufficient to describe the void fraction and velocity distribution a mesh of 60µm has chosen in order to be sure that the results are correct.

2.2. Mathematical formulation

2.2.1. The bubble dispersion problem

Lee *et al.* [22], Abdelouhaed *et al.* [23] and Hreiz *et al.* [8] experimentally visualized and measured the void fraction distribution in the electrolyte in a cell under forced convection[22] and not net flow configuration cell [8][23]. They all reported that the bubbles were spread into the electrolyte. After simulating their experiments, Albelouhed et *al.* [23] observed that classical models of lift (e.g. Saffman-Mei) and drag failed to reproduce their experimental results. Thus, they attributed this spreading to a

lift force that have a negative coefficient. Although their model fits their experimental data, the model is questionable at least in our present configuration. Indeed, to obtain their results, a coarse mesh must be used, but for our present geometry, this coarse mesh does not satisfy all the mesh independence conditions (the reader can refer to the section 2.1). Hreiz *et al.* [24] attributed this spreading to the numerical diffusion. Hreiz *et al.* [8] modeled the same experimental study using a Euler-Lagrange model (gas is modeled as a discrete phase). They succeeded in quantitative reproduction of their experimental data by using the drag force only, but the mesh independence condition was not satisfied. The model of Mat [13] is a Euler-Euler model that succeeds in simulated results that fit experimental data but the results seem odd. They measured and calculated the diphasic boundary layer and void fraction increase with increasing electrolyte flow. Those results have been invalidated experimentally by Lee *et al.* [22] and numerically by Schillings *et al.* [11]. In addition, an increase of void fraction value triggers an increase of the cell voltage and it has been measured that increasing the electrolyte flow decreases the cell voltage. Schillings *et al.* [11] and Wedin[10] used a mixture model developed by Ishii that simulated results close to the experimental data from Boissonneau *et al.*[12]. In addition to the drag force and Saffman lift force, their closure term is composed of three terms of bubble-bubble interactions. Thus, in this study, we decided to introduce a bubble dispersion term. Indeed, a high concentration of bubbles increases the bubble collision and hence trigger of bubble diffusion from high concentration to low concentration. This phenomenon has been observed by Ham *et al.* [25]. The additional force used in this study is presented in the equation (2). As described earlier, the additional force s inspired by the force used in Marfaing *et al.* [20] and Davidson *et al.* [21]. However, in their model, the present term was multiplied by the drag coefficient. The void fraction gradient is used to traduce mathematically the diffusive nature of this force.

$$\vec{F}_{BD} = -\underbrace{\varepsilon_g \rho \frac{\boldsymbol{K_g}}{\boldsymbol{d_b}} |U_r| \vec{\nabla} \varepsilon_{\boldsymbol{g}}}_{\boldsymbol{Bubble\ \ dispersion\ \ force}} \quad (2)$$

ε is the gas or liquid fraction, the subscript k can be either O2, H2 or liq (for liquid), ρ is the density in kg m^{-3}, d_b is the bubble diameter in m, Ur is the gas phase velocity minus the liquid velocity in m s^{-1}.

By using this term, it is expected to reproduce the turbulence-like behavior of the electrolyte flow observed by Boissonneau *et al.* [12].

2.2.2. Model

The model has been designed using these hypotheses:

- The flow is isothermal, Newtonian, viscous and incompressible
- At the same time, numerical simulations were carried out in order to highlight the influence of ions on the velocity and void fraction distribution. There were only very little differences when the ions distribution was taking into account. Thus the electrolyte is considered as extremely well mixed. This hypothesis has been made also by Abdelouahed *et al.* [17] and Schillings[11].
- Oxygen, hydrogen and electrolytes are three continuum media
- The flow is considered as laminar
- The effect of the surface tension is neglected
- The bubble diameter is constant for a given current density
- The current density distribution does not affect the flow distribution [18,19]. Thus, the current density distribution is taken as uniform for the validation.

The accuracy of the two dimensional (x,y) flow hypothesis need to be discussed. Therefore, for each phase the equation set can be written:

$$\frac{\partial \varepsilon_k \rho_k}{\partial t} + \vec{\nabla} \cdot \left(\varepsilon_k \rho_k \vec{V}_k\right) = S_g \quad (3)$$

ε is the gas or liquid fraction, the subscript k can be either g (O_2, H_2) or liq, ρ is the density in kg m^{-3}, V the velocity in m s^{-1}, S_g is the term source in kg m^{-3} s^{-1}

$$\frac{\partial}{\partial t}\left(\varepsilon_k \rho_k \vec{V}_k\right) + \vec{\nabla} \cdot \left(\varepsilon_k \rho_k \vec{V}_k \vec{V}_k\right) = -\varepsilon_k \vec{\nabla} p + \vec{\nabla} \cdot \left(\varepsilon_k \bar{\bar{\tau}}\right) + \varepsilon_k \rho \vec{g} + \vec{F}_k \quad (4)$$

p is the pressure in Pa, $\bar{\bar{\tau}}$ is the stress tensor in Pa, g the gravitational acceleration in m s-2, $\vec{F}_k$ is the exchange term in N m^{-3}

The stress tensor is written as follow:

$$\bar{\bar{\tau}} = \mu_k \left[\left(\bar{\bar{\nabla}}\vec{V_k} + \bar{\bar{\nabla}}\vec{V_k}^{\,T} \right) - \frac{2}{3}\vec{\nabla} \cdot \vec{V_k} I \right] \quad (5)$$

With μ_k the viscosity of the phase k in Pa s and I the unit tensor.

$$\vec{F_k} = \vec{F_D} + \vec{F_L} + \vec{F_{BD}} \quad (6)$$

$$\vec{F_k} = \underbrace{-\frac{3}{4}\varepsilon_g \rho \frac{C_D}{d_b}|U_r|U_r}_{Drag\ force} \underbrace{- \varepsilon_g \rho C_L |U_r|\ rot(\vec{V_l})}_{Lift\ force} - \underbrace{\varepsilon_g \rho\ \frac{\boldsymbol{K_g}}{\boldsymbol{d_b}}|U_r|\vec{\nabla}\varepsilon_g}_{Bubble\ dispersion\ force} \quad (7)$$

2.3. Boundary conditions

The water electrolysis performed in Boissonneau *et al.* [12] is neither acidic or alkaline. This electrolysis is called as aqueous in this study. The supporting electrolyte is Na_2SO_4 concentrated at 50 g L^{-1}. Therefore, the reaction occurring at the anode and the cathode are Equation (8) and Equation (8), respectively.

$$H_2O_{(liq)} \rightarrow 2H^+_{(aq)} + \frac{1}{2}\ O_{2(g)} + 2e^- \quad (8)$$

$$2H_2O_{(liq)} + 2e^- \rightarrow 2OH^-_{(aq)} + \ H_{2(g)} \quad (9)$$

The quantity of produced gases is directly correlated to the current density through the Faraday's law Equation (10).

$$q_m = \mathrm{n}\frac{j\ S}{F} M_g \quad (10)$$

q_m is the mass flow of produced gas in kg s^{-1}, M_g is the molar mass of the gas kg mol^{-1}, S is the electrode surface in m^2, F is the Faraday constant 96500 C mol^{-1}, n is the ratio of the stoichiometric number of the gas and the number of electrons exchanged during the reaction.

In the two-fluids equation, for most of the authors[9–11],[17],[20],[21], the input parameters for the boundary conditions are the velocity and the void fraction. The value of the void fraction is fixed arbitrarily. According to Alexiadis[20],[21] this value does not influence the hydrodynamic of the flow. However better results have been obtained using a source term that produces gas in the cell in the vicinity of the electrodes. This method has been used by Charton *et al.* 22]. This source term is written as Equation (11):

$$S_g = \mathrm{n}\frac{j}{F \times \Delta x} M_g \quad (11)$$

Δx is the width of the first cell next to the electrode in m. For the bottom and top boundary condition, a pressure inlet (P_{Tot}=0) and pressure outlet condition (P=0) is fixed. For the other wall, a no-slip condition is fixed meaning that the velocity is set to 0 m s^{-1}.

222 **Table 1.** The boundary conditions to solve the problem

Position	Boundary conditions
x=0 H_{elec}<y<2 H_{elec}	$\overrightarrow{V_l} = \overrightarrow{V_{H2}}0$
x= 2h 0<y<3 H_{elec}	$\overrightarrow{V_l} = \overrightarrow{V_{O2}} = 0$
0<x<2h y=0	$P_{Tot} = 0$
0<x<2h y=3 H_{elec}	$P = 0$

223 *2.4. Numerical procedure*

224 The Equations (3) and (4) are solved using the commercial code, Ansys Fluent. This commercial
225 code solves equations using the finite volume method by discretizing the geometry in volume and
226 subsequently integrating the governing equation over the volume. The governing equation is
227 expressed as the following algebraic Equation (10):

$$a_p\varphi = \sum_{i}^{N} a_i\varphi + b \quad (12)$$

228
229 It is considered that the convergence is met when the residuals remain stable and when the
230 average gas and liquid velocity as well as the average gas void fraction reach the value of 10^{-3}. In
231 order to reach this convergence, for 2D simulation, the flow is initialized with a forced convection by
232 imposing a pressure at the bottom. When the convergence is reached, the obtained results is used as
233 initial guess for the bubble-driven flow.
234 Table 2 gives the inputs data for the validation of the numerical model. The input data for the
235 electrolyte was taken from the work of Isono *et al.* 23]. As the bubble diameter is taken as constant,
236 an average value has been calculated from the correlation of Schillings [11]. As aforementioned, the
237 term K in the Equation (5) is used to fit the experimental data of Boissonneau *et al.* [12]. A sensitivity
238 study has been performed to choose the parameter. The results of this study are presented in Table
239 3. The parameter K is always bigger for oxygen than hydrogen.
240
241 **Table 2.** The input values for the problem

Name	Value
Geometry inputs	
H_{elec}(mm)	40
L (mm)	30
h (mm)	1.5
H_{Tot} (mm)	120
Physical Inputs	
ρ_l (kg m^{-3})	1040
ρ_{O2} (kg m^{-3})	1.3
ρ_{H2} (kg m^{-3})	0.08
ν_l (m^2 s^{-1})	$9.97\ 10^{-7}$
Two-Phase Inputs	
d_b(μm)	for 500 A m^{-2} d_b=50μm for 1000 A m^{-2} d_b=58μm for 2000 A m^{-2} d_b=78μm

Table 3. Sensitivity study results for the parameter K

500 A m^{-2}	**1000 A m^{-2}**	**2000 A m^{-2}**
K_{O2}/d=10.5	K_{O2}/d =9	K_{O2}/d =5
K_{H2}/d=5	K_{H2}/d =4	K_{H2}/d =2.5

In order to use the current model to other design, the Vaschy-Buckingham has been used and the sensitivity of the K parameter to dimensionless groups has been calculated Equation (11) to Equation (14).

$$Re_G = \frac{\rho_l \ V_G \quad H_{elec}}{\mu_L} \tag{13}$$

$$Fr_G = \frac{g \ H_{elec}}{{V_G}^2} \tag{14}$$

$$r^* = \frac{d}{2 \ H} \tag{15}$$

$$h^* = \frac{h}{H} \tag{16}$$

Therefore, the following correlation Equation (15) was used to calculate the K parameter. However, this correlation was used for height in the order of 10 centimetres and for FrG number higher than 10^5.

$$\frac{K}{V_G \ H} = 0.197 \ {Re_G}^{0.108} + 0.5 \ {r^*}^{0.124} + 0.668 \ {h^*}^{-0.408} + 0.000323 \ {Fr_G}^{0.661} + 0.375 \tag{17}$$

3. Results

The experimental data of Boissonneau *et al.* [12] are the liquid velocity at three locations: 5mm before the electrodes (y=35mm), at the mid section of the electrodes (y=60mm) and 5mm before the ends of the electrodes (y=75mm). Figures 2-4 present the results of the current study and the experimental data. At the entrance of the channel, a Poiseuille liquid velocity distribution is observed and this distribution is flattened at the center (also called bulk). The exchange of momentum between the gas phases and the liquid phase is well observed next to the anode and cathode. It can be noticed that the peak induced by hydrogen is bigger than the oxygen because the injected volume of hydrogen is two times bigger than oxygen one. The fact is that in the bulk, a plateau is observed due to bubble induced turbulence [12]. Those figures allow the comparison of the current numerical results with experimental data. The "Abdelouahed-like" model is a model that uses the same method as presented in Abdelouahed *et al.* [23]. In their study [23], the authors used the lift coefficient to fit their simulated data with their experimental values. They showed that a negative coefficient permits a good agreement between their measurements and predicted values. In the present study, a sensitivity study was performed to have the coefficient that fits the most the experimental data from Boissonneau *et al.* [12]. First of all, the numerical results for all the models show some discrepancies with the experimental data. Schilling's model and Abdelouahed-like model accurately predict the

velocity distribution on the cathode side, but the accuracy of the simulated data drops on the anode side. The Figure (2) shows that the "Abdelouahed-like" model describes the anode side and cathode side velocity distribution with accuracy, but the bulk velocity distribution shows larger errors. However, as shown in the Figures (3) and (4), the more the current density increases, the less precise the model is.

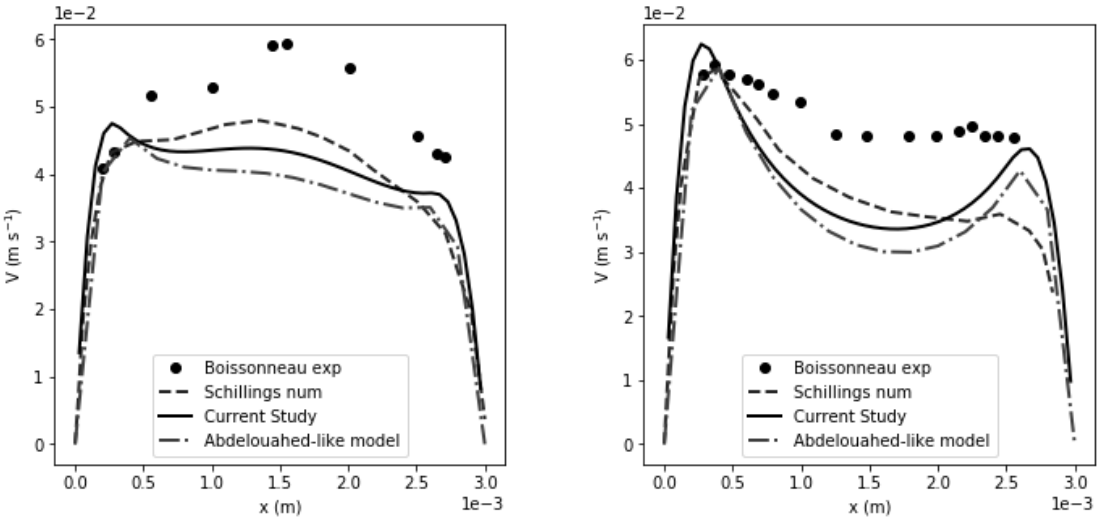

Figure 3. Result of the liquid velocity in different models at j=500 A m^{-2} (a) at y=60mm and (b) at y=75mm. The black dots are the data from Boissonneau *et al.*[12], the black solid line with grey dots is the numerical results of the Schilling model[11], the dotted line with yellow dots is a model using the method of Abdelouahed *et al.*[23]. Finally, the grey solid line with grey dots is the results from the current study with 2D approximation.

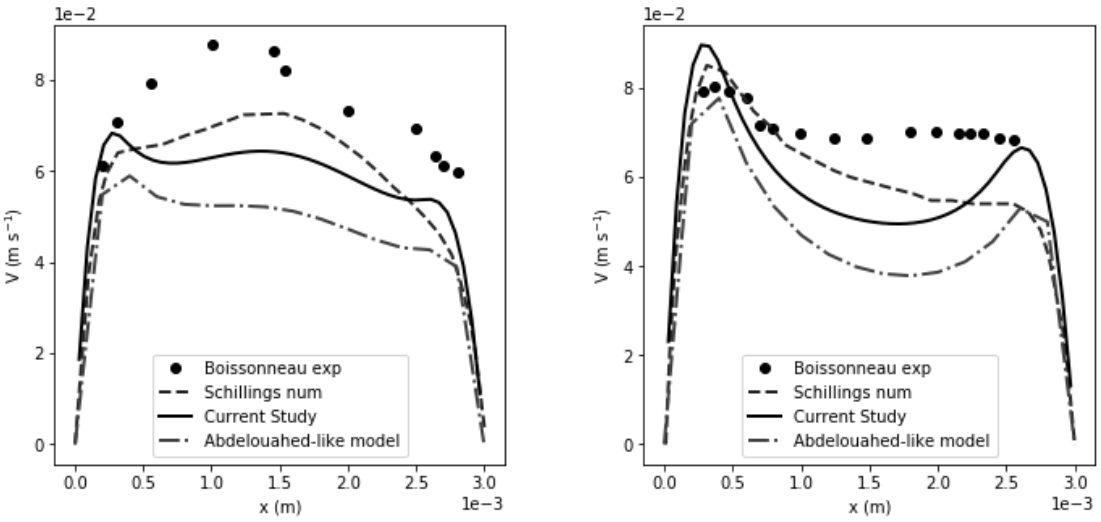

Figure 4. Results of the liquid velocity in different models at j=1000 A m-2 (a) at y=60mm and (b) at y=75mm. The black dots are the data from Boissonneau *et al.*[12], the black solid line with grey dots is the numerical results of the Schilling model[11], the dotted line with yellow dots is a model using the method of Abdelouahed *et al.*[23]. Finally, the grey solid line with grey dots is the results from the current study with 2D approximation.

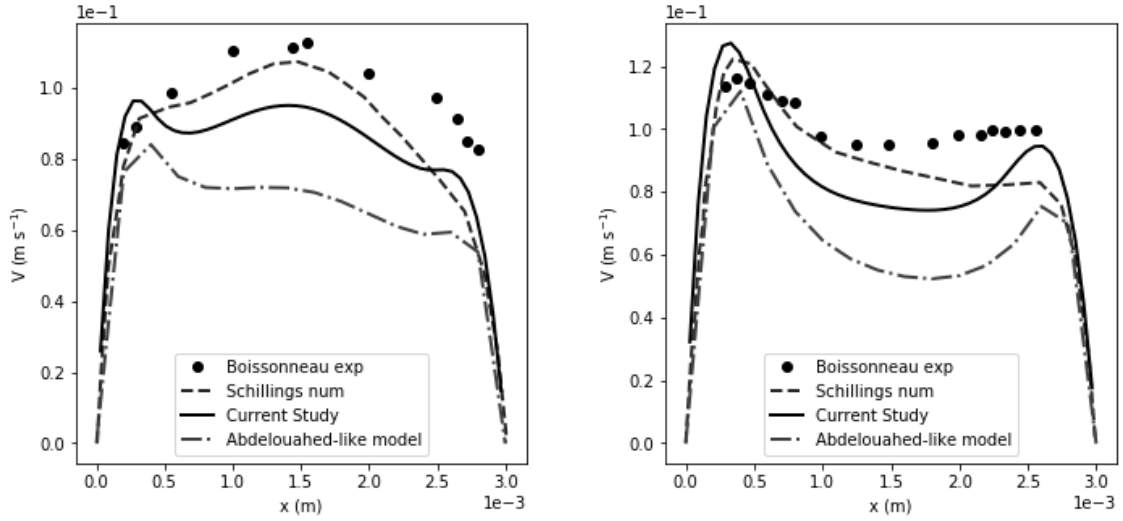

Figure 5. Result of the liquid velocity in different models at j=2000 A m-2 (a) at y=60mm and (b) at y=75mm. The dot are the data from Boissonneau *et al.*[12], the black solid line with grey dots is the numerical results of the Schilling model[11], the dotted line with yellow dots is a model using the method of Abdelouahed *et al.*[23]. Finally, the grey solid line with grey dots is the results from the current study with 2D approximation.

Figure 6 shows the void fraction evolution predicted by the current model. With an increasing current density, the diphasic boundary layer of oxygen and hydrogen and the maximum oxygen and hydrogen void fraction increase. However, there are two parameters (the current density and the bubble diameter) that change between the two cases. Therefore, the calculated evolution cannot be clearly attributed to one parameter. The prediction of this evolution depending on electrode height is very important to predict the current density distribution. The prediction of the diphasic boundary layer thickness is also an essential output parameter because the electrolyte conductivity decreases with the void fraction.

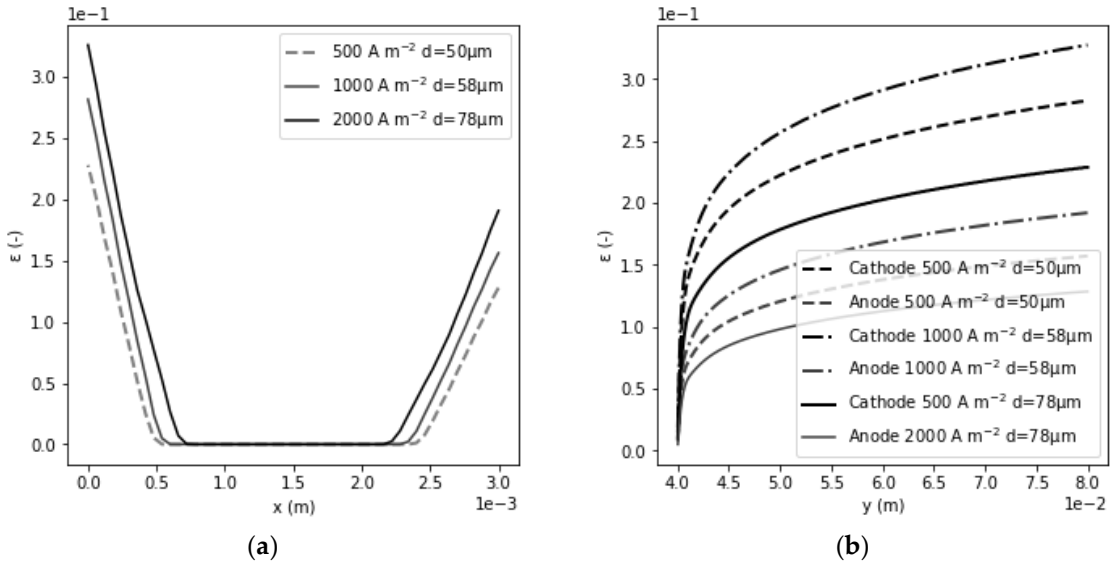

Figure 6. Void fraction evolution depending on the electrolyte width (A) and electrode height (B) for the three current density 500 A m^{-2}, 1000 A m^{-2} and 2000 A m^{-2}.

Table 4. Maximum liquid velocity at cathode and anode sides, maximum oxygen and hydrogen void fraction and hydrogen and oxygen diphasic boundary layer for the three cases

	$V_{max\ liq\ cath}$ (m s^{-1})	$V_{max\ liq\ an}$(m s^{-1})	$\varepsilon_{max\ H2}$	$\varepsilon_{max\ O2}$	δ_{H2} (µm)	δ_{O2} (µm)	R(ε)/R
500 A m^{-2}	7.8 10^{-2}	4.8 10^{-2}	0.23	0.13	515	600	1.032
1000 A m^{-2}	9 10^{-2}	6.8 10^{-2}	0.28	0.16	566	677	1.043
2000 A m^{-2}	1.25 10^{-1}	9.1 10^{-2}	0.33	0.19	690	800	1.057

Table 4 summarizes the results of the study. It must be noticed that the diphasic boundary layer of hydrogen is thinner than the oxygen one. These results are compared with the those of Schillings[11]. In Schillings' study, the authors performed a dimensional study and found that the diphasic boundary layer depends on one dimensionless group, which presented in Equations (18) and (19) (called Rayleigh-like number). The current results correspond well to the Schillings prediction. Thus, when the radius increases, the diphasic boundary layer increases and when the equivalent injection gas velocity increases, the boundary layer decreases.

$$\log\left(\frac{\delta}{h}\right) = -0.25\log(Ra) + Cst \tag{18}$$

$$Ra = \frac{\nu\ U_g h^5}{g\ r^6\ H_{elec}} \tag{19}$$

The conductivity evolution depending on electrolyte gas content is well described by the Bruggeman correlation (Equation (17)). This correlation has been compared to experimental results in Hine *et al.*[6].

$$\frac{\sigma(\varepsilon)}{\sigma_0} = (1-\varepsilon)^{1.5} \tag{19}$$

σ_0 the gas-free electrolyte conductivity in S m^{-1}

Thus, the ohmic resistance presented in Equation (1) becomes Equation (19):

$$R(\varepsilon) = \frac{\delta_{H2}}{\sigma_0\ (1-\varepsilon)^{1.5}} + \frac{2h-\delta_{O2}-\delta_{H2}}{\sigma_0} + \frac{\delta_{O2}}{\sigma_0\ (1-\varepsilon)^{1.5}} \tag{20}$$

In order to compare biphasic system with a gas-free system, the previous resistance can be divided by the hypothetical gas-free resistance.

$$\frac{R(\varepsilon)}{R} = \frac{\frac{\delta_{H2}}{\sigma_0\ (1-\varepsilon)^{1.5}} + \frac{2h-\delta_{O2}-\delta_{H2}}{\sigma_0} + \frac{\delta_{O2}}{\sigma_0\ (1-\varepsilon)^{1.5}}}{\frac{2h}{\sigma_0}} \tag{1}$$

Table 4 shows that with an increasing current density and bubble radius, the resistance increases. This statement shows that the bubble management is an important issue.

5. Conclusions

In this study, a two-fluid multi-physics model with a new bubble transfer description has been proposed. This new description allows a good accord with the Boissonneau *et al.* [12] experimental velocity profiles. It has been found out that the bubble dispersion force allows a good agreement with experimental data and a better numerical convergence than the one obtained without with this additional force. That observation correlate with the studies of other studies such as Panicker *et al.* [18]. From the numerical point of view, the grid resolution remains a problem because even if the dispersion bubbles force improves the results, there still exists a maximum grid resolution. This maximum grid resolution could lead to some inaccuracy if the fluid viscosity is too small or if the electrolyte width is too thin. Further calculation must be performed to suppress this limitation by using a 3D geometry [16]. From the physical point of view, it can be concluded that the bubble radius and current density are two important parameters that influence the hydrodynamic. However, further calculation must be performed to characterize properly the output parameters sensitivities (velocity, void fraction etc.) to the current density and bubble diameter.

Author Contributions: "Conceptualization, Damien Le Bideau and Philippe Mandin ; methodology, Damien Le Bideau and Philippe Mandin .; software, Damien Le Bideau and Philippe Mandin; validation, Damien Le Bideau and Philippe Mandin.; investigation, Damien Le Bideau and Philippe Mandin ; data curation, Damien Le Bideau and Philippe Mandin; writing—original draft preparation, Damien Le Bideau and Philippe Mandin; writing—review and editing, Philippe Mandin and Mohamed Benbouzid.; visualization, Philippe Mandin and Mohamed Benbouzid.; supervision, Philippe Mandin and Mohamed Benbouzid.; project administration, Philippe Mandin ; funding acquisition, Philippe Mandin. All authors have read and agreed to the published version of the manuscript.

Funding: This research was funded by the national association ADEME and Bretagne Region (France)

Acknowledgments: We would like to deeply thank the national association ADEME for funding our research and the Bretagne region to support our research.

Conflicts of Interest: The authors declare no conflict of interest

References

(1) H. Schäfer; M. Chatenet. Steel: The Resurrection of a Forgotten Water-Splitting Catalyst. *ACS En. Lett.* **2018**, *3*, 574–591.

(2) M. J. Lavorante; J. I. Franco. Performance of Stainless Steel 316L Electrodes with Modified Surface to Be Use in Alkaline Water Electrolyzers. *Int J. Hydrogen Energy* **2016**.

(3) C. Bocca; G. Cerisola; A. Barbucci; E. Magnone. Oxygen Evolution on Co2O3 and Li!Doped Co2O3 Coated Electrodes in an Alkaline Solution. *Int. J. Hydrog. Energy* **1999**, *24*, 699–707.

(4) Babu, R.; Das, M. K. Experimental Studies of Natural Convective Mass Transfer in a Water-Splitting System. *Int J. Hydrogen Energy* **2019**, *44* (29), 14467–14480. https://doi.org/10.1016/j.ijhydene.2019.04.043.

(5) Tobias, C. W. Effect of Gas Evolution on Current Distribution and Ohmic Resistance in Electrolyzers. *J. Electrochem. Soc.* **1959**, *106* (9), 6.

(6) Hine, F. Bubble Effects on the Solution IR Drop in a Vertical Electrolyzer Under Free and Forced Convection. *J. Electrochem. Soc.* **1980**, *127* (2), 292. https://doi.org/10.1149/1.2129658.

(7) Philippe, M.; Jérôme, H.; Sebastien, B.; Gérard, P. Modelling and Calculation of the Current Density Distribution Evolution at Vertical Gas-Evolving Electrodes. *Electrochim. Acta* **2005**, *51* (6), 1140–1156. https://doi.org/10.1016/j.electacta.2005.06.007.

(8) Hreiz, R.; Abdelouahed, L.; Fünfschilling, D.; Lapicque, F. Electrogenerated Bubbles Induced Convection in Narrow Vertical Cells: PIV Measurements and Euler–Lagrange CFD Simulation. *Chem. Eng. Sci.* **2015**, *134*, 138–152. https://doi.org/10.1016/j.ces.2015.04.041.

(9) Dahlkild, A. A. Modelling the Two-Phase Flow and Current Distribution along a Vertical Gas-Evolving Electrode. *J. Fluid. Mech.* **2001**, *428*, 249–272. https://doi.org/10.1017/S0022112000002639.

(10) Wedin, R.; Dahlkild, A. A. On the Transport of Small Bubbles under Developing Channel Flow in a Buoyant Gas-Evolving Electrochemical Cell. *Ind. Eng. Chem. Res.* **2001**, *40* (23), 5228–5233. https://doi.org/10.1021/ie001073u.

(11) Schillings, J.; Doche, O.; Deseure, J. Modeling of Electrochemically Generated Bubbly Flow under Buoyancy-Driven and Forced Convection. *Int. J. Heat Mass Transf.* **2015**, 292–299.

(12) Boissonneau, P.; Byrne, P. An Experimental Investigation of Bubble-Induced Free Convection in a Small Electrochemical Cell. *J. Appl. Electrochem.* **2000**, *30*, 767–775.

(13) Aldas, K.; Pehlivanoglu, N.; Mat, M. D. Numerical and Experimental Investigation of Two-Phase Flow in an Electrochemical Cell. *Int. J. Hydrogen Energy* **2008**, *33* (14), 3668–3675. https://doi.org/10.1016/j.ijhydene.2008.04.047.

(14) Mat, M. A Two-Phase Flow Model for Hydrogen Evolution in an Electrochemical Cell. *Int. J. Hydrogen Energy* **2004**, *29* (10), 1015–1023. https://doi.org/10.1016/j.ijhydene.2003.11.007.

(15) Riegel, H.; Mitrovic, J.; Stephan, K. Role of Mass Transfer on Hydrogen Evolution in Aqueous Media. *J. Appl. Phys.* 8.

(16) Panicker, N.; Passalacqua, A.; Fox, R. O. On the Hyperbolicity of the Two-Fluid Model for Gas–Liquid Bubbly Flows. *App* **2018**, *57*, 432–447. https://doi.org/10.1016/j.apm.2018.01.011.

(17) Abdelouahed, L.; Hreiz, R.; Poncin, S.; Valentin, G.; Lapicque, F. Hydrodynamics of Gas Bubbles in the Gap of Lantern Blade Electrodes without Forced Flow of Electrolyte: Experiments and CFD Modelling. *Chem. Eng. Sci.* **2014**, *111*, 255–265. https://doi.org/10.1016/j.ces.2014.01.028.

(18) Abdelouahed, L. Gestion optimale du gaz électrogénéré dans un réacteur d'électroréduction de minerai de fer. PhD Thesis, Université de Lorraine, Nancy.

(19) Schillings, J. Etude numérique et expérimentale d'écoulements diphasiques: application aux écoulements à bulles générées par voie électrochimique. PhD Thesis, Université Grenoble Alpes, Grenoble, 2018.

(20) Alexiadis, A.; Dudukovic, M. P.; Ramachandran, P.; Cornell, A.; Wanngård, J.; Bokkers, A. Liquid–Gas Flow Patterns in a Narrow Electrochemical Channel. *Chem. Eng. Sci.* **2011**, *66* (10), 2252–2260. https://doi.org/10.1016/j.ces.2011.02.046.

(21) Alexiadis, A.; Dudukovic, M. P.; Ramachandran, P.; Cornell, A.; Wanngård, J.; Bokkers, A. On the Electrode Boundary Conditions in the Simulation of Two Phase Flow in Electrochemical Cells. *Int. J. Hydrogen Energy* **2011**, *36* (14), 8557–8559. https://doi.org/10.1016/j.ijhydene.2011.04.149.

(22) Charton, S.; Rivalier, P.; Ode, D.; Morandini, J.; Caire, J. P. Hydrogen Production by the Westinghouse Cycle: Modelling and Optimization of the Two-Phase Electrolysis Cell; Bologna, Italy, 2009; pp 11–22. https://doi.org/10.2495/ECOR090021.

(23) Isono, T. Density, Viscosity, and Electrolytic Conductivity of Concentrated Aqueous Electrolyte Solutions at Several Temperatures. Alkaline-Earth Chlorides, Lanthanum

408 Chloride, Sodium Chloride, Sodium Nitrate, Sodium Bromide, Potassium Nitrate, Potassium
409 Bromide, and Cadmium Nitrate. *J. Chem. Eng. Data* **1984**, *29* (1), 45–52.
410 https://doi.org/10.1021/je00035a016.

411

412